

RSC Advances



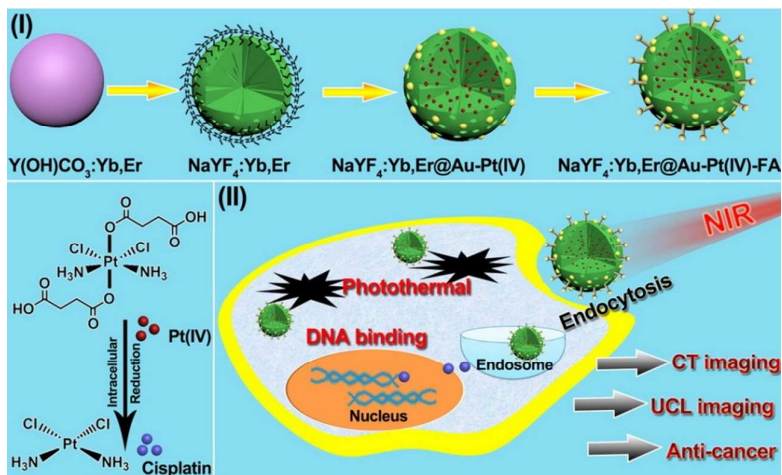
This is an *Accepted Manuscript*, which has been through the Royal Society of Chemistry peer review process and has been accepted for publication.

Accepted Manuscripts are published online shortly after acceptance, before technical editing, formatting and proof reading. Using this free service, authors can make their results available to the community, in citable form, before we publish the edited article. This *Accepted Manuscript* will be replaced by the edited, formatted and paginated article as soon as this is available.

You can find more information about *Accepted Manuscripts* in the [Information for Authors](#).

Please note that technical editing may introduce minor changes to the text and/or graphics, which may alter content. The journal's standard [Terms & Conditions](#) and the [Ethical guidelines](#) still apply. In no event shall the Royal Society of Chemistry be held responsible for any errors or omissions in this *Accepted Manuscript* or any consequences arising from the use of any information it contains.

Mesoporous $\text{NaYF}_4:\text{Yb,Er}@\text{Au-Pt(IV)}\text{-FA}$ up-conversion nanoparticles has been designed for dual-modal imaging-guided anti-cancer therapy. Under 980 nm irradiation, the platform shows excellent inhibition to cancer cells due to the synergistic photothermal/chemo- therapy.



ARTICLE

Mesoporous NaYF₄:Yb,Er@Au-Pt(IV)-FA nanospheres for dual-modal imaging and synergistic photothermal/chemo- anti-cancer therapy

Cite this: DOI: 10.1039/x0xx00000x

Received 00th January 2012,
Accepted 00th January 2012

DOI: 10.1039/x0xx00000x

www.rsc.org/

Ruichan Lv, Guixin Yang, Fei He, Yunlu Dai, Shili Gai*, and Piaoping Yang*

In this report, mesoporous NaYF₄:Yb,Er@Au-Pt(IV)-FA up-conversion nanoparticles (UCNPs) has been designed by attaching Au NPs and Pt(IV) pro-drugs on the surface of PEI hydrogel modified mesoporous NaYF₄:Yb,Er nanospheres. The finally modified folic acid (FA) molecules improve the receptor-mediated endocytosis. Because of the doped rare earth ions in the host matrix, the as-synthesized platform exhibits excellent up-conversion luminescence (UCL) imaging and computed X-ray tomography (CT) imaging properties. Diverse methods including MTT assay, hemolysis experiment, and live/dead cell analysis were employed to evaluate the biocompatibility and ablation efficacy of the as-synthesized platform. It is found that cytotoxicity of the platform can be tuned by eliminating the axial ligands reductively during intracellular endocytosis. Especially, under 980 nm near-infrared (NIR) irradiation, the platform shows excellent inhibition to cancer cells due to the synergistic photothermal injury to enzymes and membrane integrity combined with the DNA binding of activated Pt(II) to avoid the cell passage. The developed nanocomposite may thus be a promising imaging-guided synergistic anti-cancer platform.

1. Introduction

For drug delivery systems (DDSs), when referred to photosensitive therapy, two irrelevant lights are commonly utilized to achieve diagnosis and effective therapy because of the limited penetration depth of conventional ultraviolet and visible light, thus it is difficult for real-time assessment of the anti-cancer therapeutic effect.¹⁻³ Multi-modal imaging is an effective tool to detect and manage the malignant cancer sites which could synergistically combine the penetration, sensitivity and resolution for diagnosis.^{4,5} CT imaging is one of the most common clinic diagnostic techniques due to the deep tissue penetration and high-resolution 3D structure details.^{6,7} Although the high resolution of CT imaging is important, there is a limitation due to its low sensitivity, especially when used for tumor-imaging with small density differences. For single UCL fluorescence, it is sensitive but with poor tissue penetration. Thus, finding effective synergistic imaging-guided anti-cancer platform and strategy induced by a single light is an extremely important subject in this field.⁸⁻¹¹

The novel NIR irradiation located at the optical transmission window with lower absorbance of endogenous chromophores (hemoglobin and melanin) by living subjects also has significant advantages such as deep penetration, high detection sensitivity, and decreased background signal.¹²⁻¹⁷ Meanwhile, NIR irradiation has appealing properties for drug delivery application which could emit visible light to track the tumor site through two-/multi-photon energy transfer process, and the obtained high energy as the donors could transfer to the photosensitive agents.¹⁸⁻²¹ This amazing photo-conversion

process allows up-conversion nanoparticles (UCNPs) to serve as an effective single NIR light irradiated mediator for their extensive anti-cancer therapeutic applications with remote regulation of photosensitive activation, including bio-imaging and targeted delivery of drug molecules to cancer sites.²²⁻²⁴

Cis-dichlorodiammineplatinum (II) (denoted as cisplatin) is one of the most widely used anticancer drugs which is effective and could be clinically used to inhibit head and neck, esophageal, bladder, cervical, and non-small cell lung cancer, etc.²⁵⁻²⁸ Just like other chemo-therapeutic drug molecules, small molecular cisplatin which lacks of controlled release with very low intracellular reaction efficiency may have serious side effect to normal cells and thus could introduce complications, such as nausea, hearing damage, peripheral nerve impairment, and irreversible nephrotoxicity.^{29,30} Researchers have tried to find new drug candidates and introduce DDSs to decrease the chemotherapeutic side effect to achieve the targeted anti-tumor therapy.^{31,32} Pt(IV) compound has been proposed as an attractive alternative to Pt(II) complex because their inertness in the normal cells and body fluid. However, it seems the anti-cancer efficiency is not as high as predicted because Pt(IV) pro-drugs can only be changed to Pt(II) species by reduction in the presence of intracellular biological reducing agents, such as glutathione and ascorbic acid or *via* acid hydrolysis. Meanwhile, the single chemo-therapeutic mode impulses bodies resistance to drugs, and the medicines lose drug potency with prolonging times.³³ Thus, versatile synergistic photothermal/photodynamic anti-cancer platforms are developed.³⁴⁻⁴² Gold nanoparticles could receive the broad UCL emissions by fluorescence resonance energy transfer

(FRET) from the UCL hosts because there is an intense absorption located in the visible region.^{41–45} Meanwhile, they demonstrate strong absorption with relatively higher molar extinction coefficient and photothermal conversion efficiency.^{47–51} When Au nanostructures were utilized, the generated intensive photothermal effect could destruct the cell membrane integrity and enzymes to interference DNA synthesis.^{52,53} If the photothermal effect is combined with the DNA binding caused by chemo- effect of Pt(II) species through fabricating functional structure, it is expected to obtain outstanding therapeutic efficiency because it could yield a synergistic efficacy which is higher than the sum of individual efficacy.

Herein, dual-modal imaging-guided platform of NaYF₄:Yb,Er@Au-Pt(IV)-FA UCNP was designed for synergistic photothermal/chemo- therapy with non-toxicity to normal cells. Pt(IV) as the targeted anti-cancer pro-drugs was synthesized through initial oxidization and subsequent reaction with succinic anhydride. Mesoporous NaYF₄:Yb,Er nanospheres was prepared through hydrothermal process using Y(OH)CO₃:Yb,Er as the precursor. Large amount of PEI hydrogel on the surface of 90-nm NaYF₄:Yb,Er serves as the drug carrier which could covalently conjugate the negative Au nanospheres and Pt(IV) molecules through the physical attraction and chemical functional conjunction. MTT assay, hemolysis experiment, and live/dead cell analysis were employed to evaluate the drug molecule and carrier to the viability of normal cells and cytotoxicity to cancer cells. Moreover, the doped rare earth ions in the composite make the material have good UCL imaging and CT imaging properties. The results proved that the NaYF₄:Yb,Er@Au-Pt(IV)-FA platform has dual-modal imaging properties and synergistic photothermal and chemo- therapeutic effect to cancer cells.

2. Experimental section

2.1 Chemicals and materials

All the reagents used in this research are purchased and utilized directly without any further purification, including Y₂O₃, Yb₂O₃, and Er₂O₃ (Sinopharm Chemical Reagent Co., Ltd., China), hydrogen peroxide (H₂O₂), urea, nitric acid (HNO₃), HAuCl₄·3H₂O, sodium citrate (Na₃Cit), tannin acid, dimethyl sulfoxide (DMSO) (from Beijing Chemical Corporation, China), sodium chloride (NaCl), phosphate buffered saline (PBS), glutaraldehyde (from Tianjin Kernel Chemical Co., Ltd., China), cisplatin, succinic anhydride, polyethyleneimine (PEI), 1-(3-dimethylaminopropyl)-3-ethylcarbodiimide hydrochloride (EDC), and Nhydroxysuccinimide (NHS), folic acid (FA), 3-4,5-dimethylthiazol-2-yl-2,5-diphenyl tetrazolium bromide (MTT), 4',6-diamidino-2-phenylindole (DAPI), calcein AM, propidium iodide (PI), trypan blue (from sigma-Aldrich).

2.2. Synthesis

Synthesis of gold nanospheres. The Au nanospheres with a mean size of 10 nm were synthesized according to the literature.⁵⁴ Instead of using the strong reduction of NaBH₄, the HAuCl₄·3H₂O was reduced by citrate in the presence of tannic acid. Briefly, 5 mL of HAuCl₄·3H₂O (25 mM) was mixed with 30 mL deionized water, and then sodium citrate (0.2 g) and tannic acid (0.03 g) were added swiftly. The colorless transparent solution was changed to dark purple red immediately, and then the solution was kept stirring at 60 °C for 4 h. The solution was then kept cold and used within several days.

Synthesis of Pt(IV) pro-drug. The Pt(IV) pro-drug of *c,c,t*-Pt(NH₃)₂Cl₂(OOCCH₂CH₂COOH)₂ (denoted as Pt(IV)) was synthesized through a two-step process according to the literature.⁵⁵ The intermediate product of *c,c,t*-Pt(NH₃)₂Cl₂(OH)₂ was firstly synthesized. Typically, cisplatin (2.5 g) was suspended into 125 mL of deionized water, 87.5 mL of H₂O₂ (30%) was added and stirred at 50 °C for 1 h. The product was then isolated and recrystallized. Then, *c,c,t*-Pt(NH₃)₂Cl₂(OH)₂ was obtained after washed with cold deionized water, ethanol and acetone. 0.7 g of synthesized *c,c,t*-Pt(NH₃)₂Cl₂(OH)₂ was dissolved in DMSO (5 mL) with succinic anhydride (2 g) added, and the mixture was stirred at 70 °C for 24 h. Finally, the pale yellow *c,c,t*-Pt(NH₃)₂Cl₂(OOCCH₂CH₂COOH)₂ was obtained.

Synthesis of Y(OH)CO₃:Yb/Er. The precursor of Y(OH)CO₃:Yb/Er was synthesized through co-precipitation method.⁵⁶ Note that the sizes could be easily controlled by adjusting the initial pH values. Briefly, 1 mol L⁻¹ of Ln(NO₃)₃ (Ln = Y, Yb, and Er) solutions were firstly prepared by dissolving rare earth oxides into nitric acid with continuous heating. Then, the calculated Ln(NO₃)₃ (81%Y, 18%Yb, and 1%Er) was added into 50 mL of deionized water, and then 3 g of urea was added with stirring. When the solution was transparent, the mixture in the beaker was kept heating in a water bath at 90 °C for 3 h, and the precipitation were collected after centrifugation and drying at 60 °C for 12 h.

Synthesis of mesoporous NaYF₄:Yb/Er-PEI. In order to further obtain the better UCL host of a lanthanide fluoride with favourable dispersity, porous structure, and functional groups, the precursor was dissolved into 20 mL of deionized water and pre-mixed with 5 mL of PEI (50 mg mL⁻¹) under ultrasonic treatment (10 min) and stirred for 2 h. After that, 4 mmol of NaBF₄ was added into the mixture, and they were kept stirring for another 30 min. The uniform solution was sealed into a 40 mL of kettle and kept at 150 °C for 3 h. NaYF₄:Yb,Er with PEI hydrogel shell was obtained with centrifugation and drying.

Synthesis of NaYF₄:Yb/Er@Au-Pt(IV). 1 mL of as-prepared gold nanospheres solution was firstly added into 0.15 mg of NaYF₄:Yb,Er dispersed 20 mL of deionized water. After stirring for 2 h, the mixture was washed three times with deionized water and centrifuged with 6000 rpm for 5 min. The pale purple precipitation was acquired due to the successful conjunction of gold nanospheres. Then, the precipitation was dispersed into 20 mL of water and mixed with 30 mg of as-prepared Pt(IV) pro-drug, the NaYF₄:Yb/Er@Au-Pt(IV) was obtained after final centrifugation. The supernatant was kept for further ICP-MS in order to calculate the loading amount of Pt(IV).

FA modified NaYF₄:Yb/Er@Au-Pt(IV)-FA. Typically, 0.15 g of NaYF₄:Yb/Er@Au-Pt(IV) was dissolved into 20 mL of deionized water. 1 mL of FA (10 mg mL⁻¹), 1 mL of NHS (2 mg mL⁻¹), 1 mL of EDC (6 mg mL⁻¹) were kept stirring for 2 h in dark, and then the solution was added into the solution of NaYF₄:Yb/Er@Au-Pt(IV) with continuous stirring for another 12 h in dark. The pale brown product was collected by centrifugation and washed with water three times to remove the free FA molecules. After drying at 60 °C for 12 h, the yellow brown powders are NaYF₄:Yb/Er@Au-Pt(IV)-FA UCNPs.

2.3 Characterization

Powder X-ray diffraction (XRD) measurements were carried out on a Rigaku D/max TTR-III diffractometer with graphite monochromatized Cu K α radiation ($\lambda = 0.15405$ nm), and the scanning rate is 15° min⁻¹ in the 2 θ range from 20° to 80°.

Images were obtained digitally on transmission electron microscopy (TEM, FEI Tecnai G² S-Twin). Fourier Transform Infrared Spectroscopy (FT-IR) spectra were measured on a Perkin-Elmer 580B IR spectrophotometer using KBr pellet. N₂ adsorption/desorption isotherms were acquired on a Micromeritics ASAP Tristar II 3020 apparatus, and the pore size distribution was calculated by the Barrete-Jonere-Halenda (BJH) method. UCL emission spectra were obtained on Edinburgh FLS980 apparatus using a 980 nm laser diode Module (K98D08M-30W) as the irradiation source and recorded in the visible light region. The absorbance of red blood cells was measured on the microplate reader at the wavelength of 405 nm. The loading of Au nanoparticles and Pt(IV) pro-drugs on the materials was detected and calculated by the ICP-MS. The amount was calculated as follows: $M_{\text{loading}} = (M_{\text{added}} - C_{\text{Supernatant}} \times V_{\text{Supernatant}})$, where $C_{\text{Supernatant}}$ is the concentration of the detected supernatant solution and $V_{\text{Supernatant}}$ means the volume of the solution.

2.4 *In vitro* viability of drug carrier and complex

L929 fibroblast cells (about 7000 cells per well) were put in a 96-well (8×12) plate and incubated with 5% CO₂ at 37 °C, and one row (12 wells) was left with culture only as the blank control, and then incubated for 24 h to make cells attach to the wells. Then NaYF₄:Yb,Er@Au-Pt(IV) was dispersed in culture and diluted into various concentration of 500, 250, 125, 62.5, 31.3, and 15.63 μg mL⁻¹, while the concentrations of corresponding cisplatin, Pt(IV) pro-drug and complexes were diluted to 75, 37.5, 18.8, 9.4, 4.7, and 2.4 μg mL⁻¹, respectively. Then the solutions with different concentrations were added to the wells and incubated with L929 cells for another 24 h. After that, 20 μL of MTT solution (5 mg mL⁻¹) was added to each well and the cells were incubated for another 4 h at 37 °C. MTT could be reduced into formazan by the live cells, and the formazan was dissolved by DMSO. Then, DMSO (150 μL) was added to each well after the solution in the well was discarded. The absorbance at 490 nm was measured using a microplate reader for further calculation. Note that NaYF₄:Yb,Er@Au-Pt(IV) has the similar absorbance with formazan solution, and the absorbance of NaYF₄:Yb,Er@Au-Pt(IV) in culture without cells should be detected by microplate reader at 490 nm to remove the background interference to the measurement of viability.

2.5 Hemolysis assay of drug carrier and complex

Hemolysis assay of NaYF₄:Yb,Er@Au, cisplatin, and the NaYF₄:Yb,Er@Au-Pt(IV) was carried out to evaluate the potential biocompatibility to the blood stream. Typically, red cells were obtained by removing the serum from human blood after washing with 0.9% (w/w) saline and centrifuged for several times until the supernatant was colourless. Subsequently, red cells were diluted with saline. 0.4 mL of diluted cells suspension was then mixed with 1.6 mL of PBS (as a negative control), 1.6 mL of deionized water (as a positive control), and 1.6 mL of UCNP suspensions with varying concentration of 500, 250, 125, 62.5, 31.3, and 15.63 μg mL⁻¹. The eight samples were shaken for a while, then kept standing for 2 h. Finally, the mixtures were centrifuged at 4000 rpm and the absorbance of the upper supernatants was measured by micro-plate reader at the wavelength of 405 nm. The hemolysis percentage was calculated as follows: Hemolysis (%) = $(A_{\text{sample}} - A_{\text{control(-)}}) / (A_{\text{control(+)}} - A_{\text{control(-)}})$, where A is the absorbance.

2.6 *In vitro* cellular uptake and UCL microscopy (UCLM) observation

HeLa cancer cell lines were utilized to detect the cellular uptake process using a confocal laser scanning microscope (CLSM, Leica SP8). In a 6-well culture plate, the HeLa cells (about 10⁵ per well) were seeded and incubated with one coverslip placed in each well overnight to obtain monolayer cells. After that, the different wells were added with NaYF₄:Yb,Er@Au-Pt(IV)-FA (1 mg mL⁻¹) at 37 °C with different incubation times for 1 h and 3 h, respectively. After each incubation time, the cells were flushed with PBS three times, and fixed with 1 mL glutaraldehyde (2.5% w/w in PBS) at 37 °C for 10 min, then rinsed with PBS three times again. 1 mL of DAPI solution (20 μg mL⁻¹ in PBS) was added and kept for another 10 min, and then rinsed three times for further detection using CLSM. For the UCL microscopy observation, the coverslip was executed with the same process except that it was detected by inverted fluorescence microscopy.

2.7 *In vitro* and *in vivo* X-ray CT imaging

The *in vitro* CT imaging experiments were performed on a Philips 64-slice CT scanner with the voltage of 120 kV. NaYF₄:Yb,Er@Au-Pt(IV)-FA was dispersed in saline and diluted to a series of concentrations of 40, 20, 10, 5, 2.5, and 1.25 mg mL⁻¹ and then placed in a line for CT imaging. The mice were first anesthetized with 10% chloral hydrate (0.03 mL g⁻¹ of mouse) by intra-peritoneal injection to perform *in vivo* CT imaging. Then, 100 μL of NaYF₄:Yb,Er@Au-Pt(IV)-FA (40 mg mL⁻¹) was intratumorally injected into the tumor-bearing mice *in situ* for better scanning.

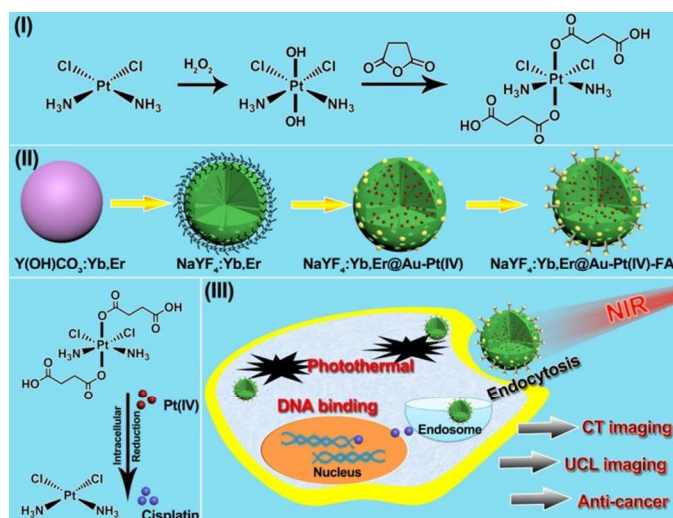
2.8 *In vitro* cytotoxicity of drug carrier and complex

The *in vitro* cytotoxicity of different materials and drugs were performed on HeLa cells using MTT assay. HeLa cells were incubated with cisplatin, Pt(IV) pro-drug, NaYF₄:Yb,Er@Au-Pt(IV)-FA nanoparticles, and NaYF₄:Yb,Er@Au-Pt(IV)-FA under NIR irradiation. The MTT assay process was carried on similar to the viability assay of L929 cells. For the live/dead cell detection process, HeLa cells were seeded in a 6-well culture plate and grown overnight as a monolayer. Then, they were incubated with different treatments: with NaYF₄:Yb,Er@Au-FA, with culture only under NIR irradiation, Pt(IV) pro-drug, NaYF₄:Yb,Er@Au-Pt(IV)-FA, cisplatin, and NaYF₄:Yb,Er@Au-Pt(IV)-FA under NIR irradiation. The pump power of NIR irradiation is 0.72 W cm⁻². Note that the materials were added and incubated for 6 h in order to complete the cell uptake, and then the irradiation was carried on just before the final dyed process. After the treatment, the wells were rinsed with PBS both dyed with calcein AM and PI, and visualized using CLSM.

3. Results and discussion

3.1 Phase, morphology, and luminescent properties

The formation of Pt(IV) pro-drugs, the synthesis process of NaYF₄:Yb,Er@Au-Pt(IV), and dual-modal imaging-guided photothermal/chemo- anti-tumor therapy application under single NIR irradiation are depicted in Scheme 1. Fig. 1 presents the XRD patterns of the Y(OH)CO₃:Yb,Er precursor, as-synthesized NaYF₄:Yb,Er after the second hydrothermal process, and NaYF₄:Yb,Er@Au-Pt(IV). As shown, there is no obvious peak in the precursor which indicates the precursor of Y(OH)CO₃:Yb,Er is amorphous. After the second-step reaction



Scheme 1 Schematic representation of the synthesis of Pt(IV) pro-drug, the anti-cancer platform, and the imaging-guided synergistic photothermal and chemo-anti-cancer process.

of the precursor with NaBF_4 , the XRD pattern of the sample is well consistent with the cubic $\text{NaYF}_4:\text{Yb,Er}$ (JCPDS: 06-0342), and the peaks are apparently strong without impurity, indicating $\text{NaYF}_4:\text{Yb,Er}$ has good crystallinity. After the Au nanospheres and Pt(IV) pro-drug are conjugated, the XRD pattern of $\text{NaYF}_4:\text{Yb,Er}@Au$ shows a new weaker peak assigned to the (111) lattice plane of cubic gold (JCPDS: 04-0784).

TEM images of the corresponding $\text{Y}(\text{OH})\text{CO}_3:\text{Yb,Er}$, $\text{NaYF}_4:\text{Yb,Er}$ and $\text{NaYF}_4:\text{Yb,Er}@Au$ are presented in Fig. 2. As shown in Fig. 2A, B, the precursor is nearly mono-dispersed with smooth surface, and the average size of the precursor is 90 nm. After the hydrothermal fluorination, uniform nanospheres with obvious pores and channels inside are obtained (Fig. 2C, D). The generation of this structure is due to the ion-exchange by the amorphous precursor with the gradually erosive NaBF_4 under the high pressure and temperature of 150 °C. Meanwhile, a large amount of $-\text{NH}-$ and $-\text{NH}_2-$ functional groups generate

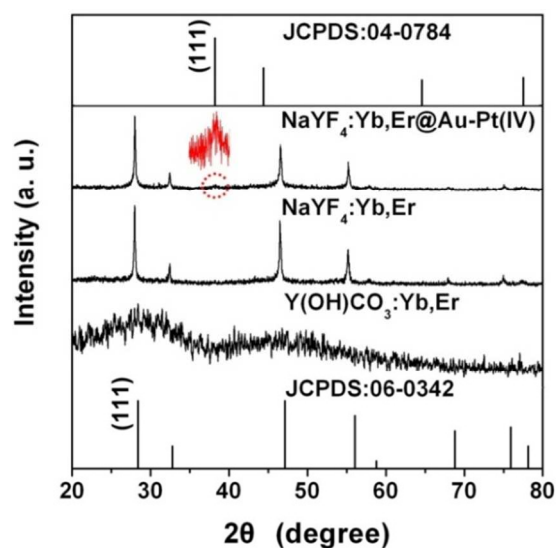


Fig. 1 XRD patterns of the precursor, $\text{NaYF}_4:\text{Yb,Er}$, $\text{NaYF}_4:\text{Yb,Er}@Au$ and $\text{NaYF}_4:\text{Yb,Er}@Au\text{-Pt(IV)}$.

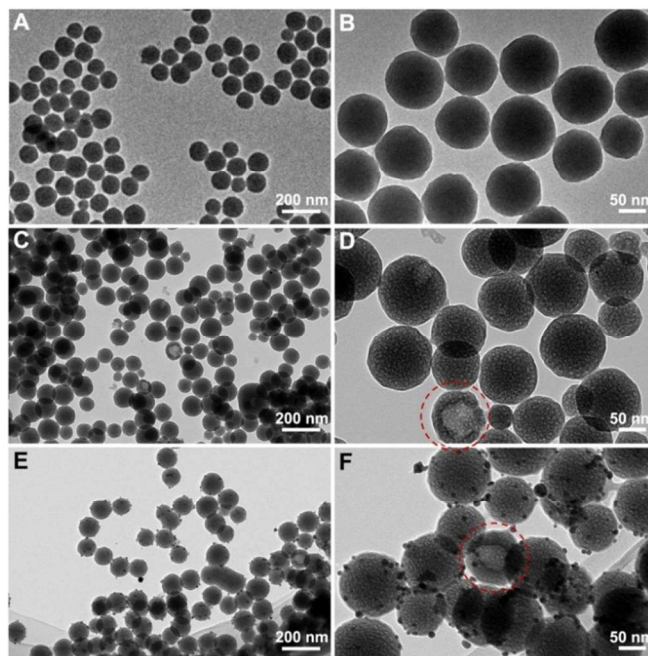


Fig. 2 TEM images with different magnification of (A, B) the precursor, (C, D) $\text{NaYF}_4:\text{Yb,Er}$, and (E, F) $\text{NaYF}_4:\text{Yb,Er}@Au$.

naturally due to added PEI which is easily to conjunct with other groups. After that, the gold nanospheres with 10 nm size is conjugated because lots of $-\text{COOH}$ and $-\text{OH}$ groups are lined on the surface of Au nanospheres during the synthesis. TEM and HRTEM image of Au spheres is shown in Fig. S1, and there is no difference between the mono-dispersed Au nanospheres and Au particles after modification due to the good chemical and physical stability of Au noble metal. Meanwhile, besides the particles modified on the surface of $\text{NaYF}_4:\text{Yb,Er}$ (Fig. 2E, F), there are almost no free particles, indicating the strong electronic absorbance between the positive $\text{NaYF}_4:\text{Yb,Er}$ nanospheres and the negative Au nanoparticles. Note that there are not many attached Au spheres considering comprehensive properties of up-conversion luminescence and photothermal property.⁵¹

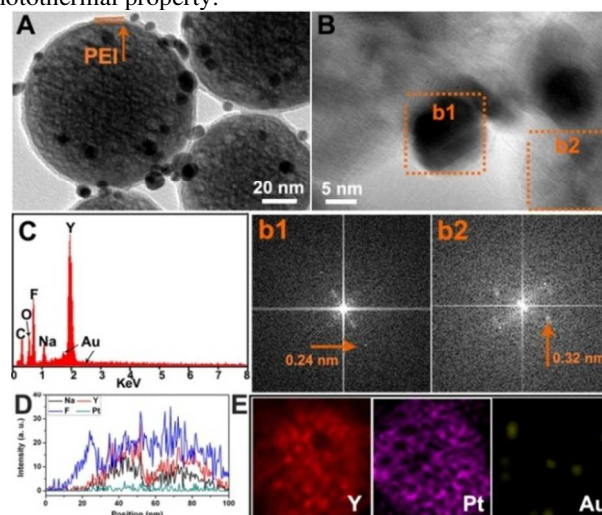


Fig. 3 (A) TEM image, (B) HRTEM image with FFT images, (C) EDS analysis, (D) EDS line profile, and (E) EDS mapping of $\text{NaYF}_4:\text{Yb,Er}@Au$ NPs.

Fig. 3A further presents TEM image of $\text{NaYF}_4:\text{Yb,Er}@Au$ with high magnification. As shown, there is an apparent thin PEI hydrogel on the surface of $\text{NaYF}_4:\text{Yb,Er}$ with the mean size of 3-4 nm. Even after Au nanospheres are modified (with few amount of Au solution), there are still a large amount of PEI groups left for the following conjunction of Pt(IV) pro-drugs while the pores and channels inside of the nanospheres also play a significant role for the next modification which is attributed to the mater design of the nanoscale particles from both the chemical and physical sides. High resolution transmission electron microscopy (HRTEM) image is shown in Fig. 3B with the corresponding fast Fourier transform (FFT) images of the corresponding regions (Fig. 3b1, b2). The 10 nm-sized nanosphere should be Au particle in b1 region which have an obvious distance of 0.24 nm assigned to (111) lattice plane of Au spheres. The apparent distance of 0.32 nm is observed in b2 region which is coincident with the (111) lattice plane of cubic $\text{NaYF}_4:\text{Yb,Er}$. The results further prove the successful conjunction of the Au nanospheres on the surface of $\text{NaYF}_4:\text{Yb,Er}$. Energy dispersive spectrometer (EDS) image in Fig. 3C indicates there are Na, Y, F, Au, C, and O elements presented in the resulted sample. Additionally, the EDS line profile (Fig. 3D) and EDS mapping (Fig. 3E) indicate the Au nanoparticles and Pt(IV) pro-drugs are well dispersed in the surface and inside of $\text{NaYF}_4:\text{Yb,Er}$.

Fig. 4 demonstrates the nitrogen adsorption/desorption isotherms and the corresponding pore volume *versus* pore size distributions of $\text{NaYF}_4:\text{Yb,Er}@Au$, and $\text{NaYF}_4:\text{Yb,Er}@Au$ with Pt(IV) pro-drug loaded, respectively. Both of the two samples exhibit typical IV-type isotherms with the main H_1

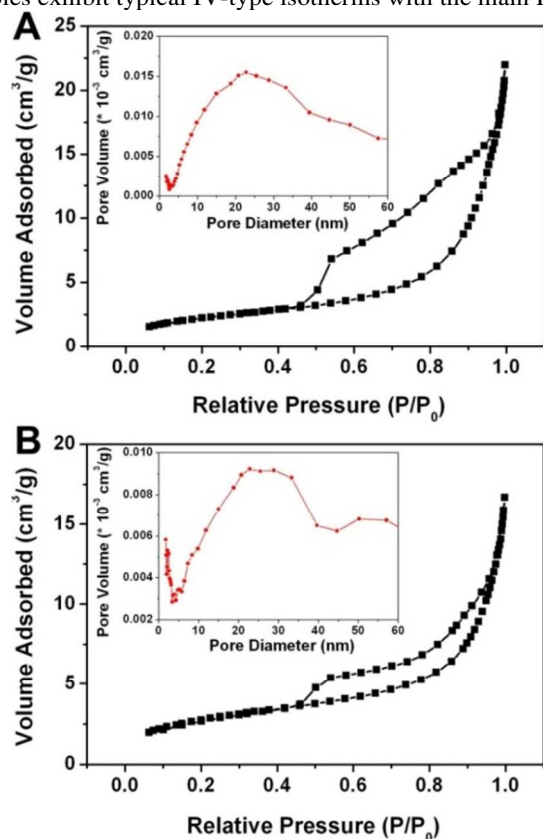


Fig. 4 Nitrogen adsorption/desorption curves and the corresponding pore size distribution (inset) of (A) $\text{NaYF}_4:\text{Yb,Er}@Au$, and (B) $\text{NaYF}_4:\text{Yb,Er}@Au\text{-Pt(IV)}$.

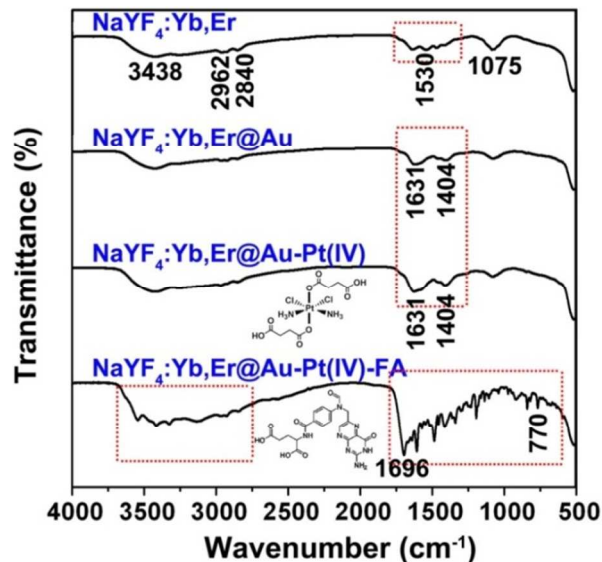


Fig. 5 FT-IR spectra of $\text{NaYF}_4:\text{Yb,Er}$, $\text{NaYF}_4:\text{Yb,Er}@Au$, $\text{NaYF}_4:\text{Yb,Er}@Au\text{-Pt(IV)}$, and (D) $\text{NaYF}_4:\text{Yb,Er}@Au\text{-Pt(IV)-FA}$.

hysteresis loop in the medium relative pressure (0.3-0.8), which indicates the mesoporous channels and pores are dispersed in the samples. Meanwhile, the BJH desorption surface of the two samples are 20.7 and 10.4 m^2g^{-1} , and the average pore sizes are 15.6 nm and 10.5 nm, respectively. There is an obvious decreased surface area between the $\text{NaYF}_4:\text{Yb,Er}@Au$ with and without Pt(IV) pro-drug loaded, which indicates the modified Pt(IV) pro-drug molecules have entered the mesopores and attracted by physical attraction and chemical conjunction.

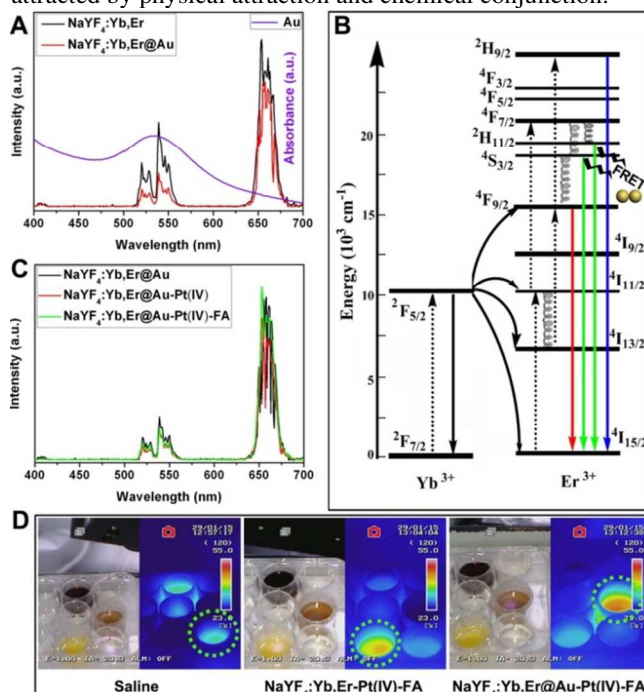


Fig. 6 (A) UCL emission spectra of $\text{NaYF}_4:\text{Yb,Er}$ with and without attached Au NPs under 980 nm irradiation and the absorbance spectrum of Au NPs solution. (B) Energy transfer process of $\text{NaYF}_4:\text{Yb,Er}$ and the FRET process with Au. (C) UCL emission spectra of $\text{NaYF}_4:\text{Yb,Er}@Au$ and $\text{NaYF}_4:\text{Yb,Er}@Au$ with Pt(IV) and FA conjugated. (D) The photographs under daylight (left) and infrared thermal images (right) of saline, $\text{NaYF}_4:\text{Yb,Er}\text{-Pt(IV)-FA}$, and $\text{NaYF}_4:\text{Yb,Er}@Au\text{-Pt(IV)-FA}$ solutions.

ARTICLE

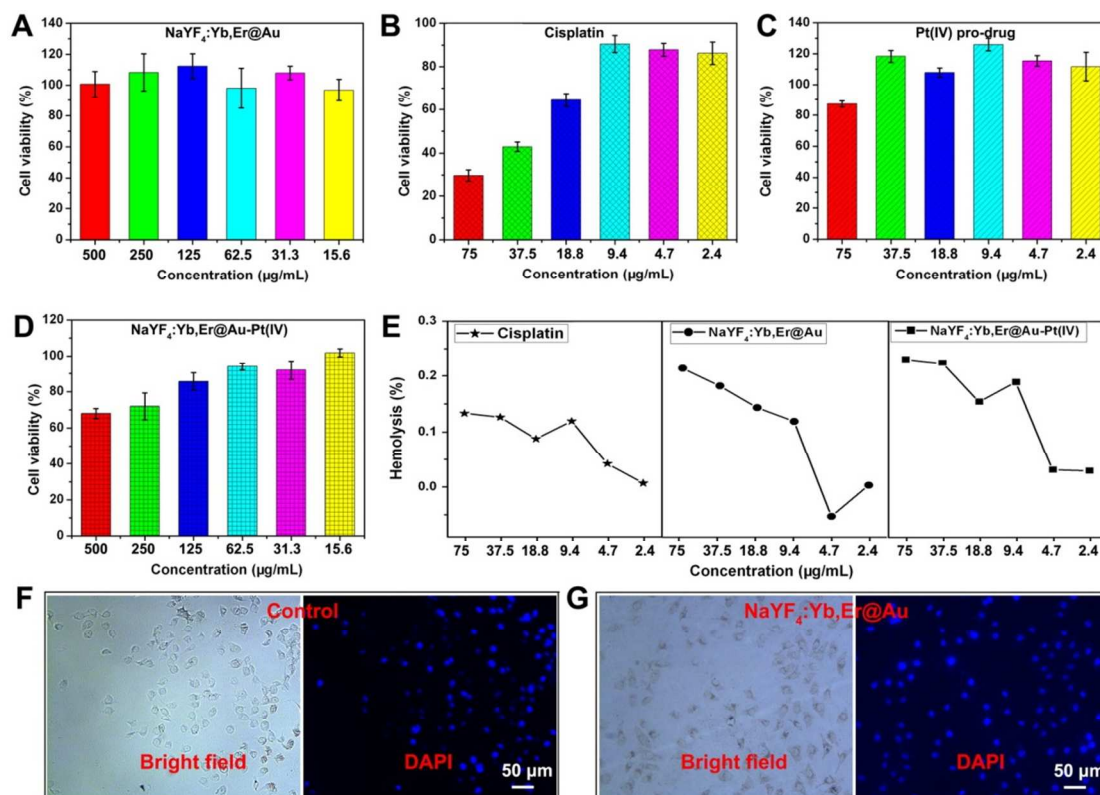


Fig. 7 Viability of L929 cells incubated with (A) NaYF₄:Yb,Er@Au, (B) cisplatin, (C) Pt(IV) pro-drug, and (D) NaYF₄:Yb,Er@Au-Pt(IV). (E) The hemolysis of cisplatin, NaYF₄:Yb,Er@Au, and NaYF₄:Yb,Er@Au-Pt(IV). The microscope images under the bright field and fluorescence field (405 nm) of L929 cells incubated (F) with culture only, and (G) with NaYF₄:Yb,Er@Au dyed by DAPI and trypan blue.

FT-IR spectra of NaYF₄:Yb,Er, NaYF₄:Yb,Er@Au, NaYF₄:Yb,Er@Au-Pt(IV), and the final NaYF₄:Yb,Er@Au-Pt(IV)-FA to further prove the successful conjugation of each step are shown in Fig. 5. Similar bands at 3438 cm⁻¹ and 1075 cm⁻¹ in the four spectra are attributed to the hydroxyl group stretching and the -YF. The spectrum of NaYF₄:Yb,Er has typical peaks at 1500-1650 cm⁻¹ and 2840-2962 cm⁻¹, which are assigned to amide bonds (-NH, -NH₂) and -CH₂ stretching vibrations from the PEI hydrogel, respectively.⁵⁷ After gold nanospheres and Pt(IV) pro-drug were modified, the typical peak at 1530 cm⁻¹ (-NH₂) disappears, while new peaks at 1631 and 1404 cm⁻¹ appear assigned to the formed -CONH- groups between the amine groups of NaYF₄:Yb,Er and the carboxyl groups and carbonyl groups of Au-Cit and *c,c,t*-Pt(NH₃)₂Cl₂(OOCCH₂CH₂COOH)₂.⁵⁸ The increased intensity of the two peaks in NaYF₄:Yb,Er@Au-Pt(IV) compared with NaYF₄:Yb,Er@Au indicates more -CONH- groups have generated. After FA molecules were modified, obvious peaks at 770-1696 cm⁻¹ and 2700-3700 cm⁻¹ assigned to the characteristic groups of FA are observed.⁵⁹ These results further demonstrate that as-synthesized gold nanospheres, Pt(IV) pro-drug, and the FA molecules have successfully conjugated on the NaYF₄:Yb,Er nanospheres.

Fig. 6A shows the emission spectra of NaYF₄:Yb,Er and NaYF₄:Yb,Er@Au samples under 980 nm excitation and the absorbance spectrum of Au nanospheres solution was also detected by the UV-vis spectrum. Three strong luminescent emissions at 520, 539, and 654 nm are assigned to the energy transfer process of ²H_{11/2}→⁴I_{15/2}, ⁴S_{3/2}→⁴I_{15/2}, and ⁴F_{9/2}→⁴I_{15/2}, respectively.⁶⁰⁻⁶⁵ Meanwhile, there is a weaker peak at 409 nm which is correspond to ²H_{9/2}→⁴I_{15/2} energy transfer process. Generally, the 409 nm due to the three- or four- photon up-conversion transfer can not be easily obtained because of the low efficiency and strong scattering, and this result indicates NaYF₄:Yb,Er is an excellent host served as the energy donor.⁶⁴ In Fig. 6A, an obvious decreased emission intensity occurs at the green region of NaYF₄:Yb,Er@Au because there is an obvious wide peak at 490-570 nm in the Au absorbance spectrum which is crossed with the UCL emission of NaYF₄:Yb,Er. There is a Förster resonance energy transfer (FRET) between the two materials, and the emission intensity of NaYF₄:Yb,Er as the donor will decrease after the Au particles as the acceptor modified. Thus, a following photothermal effect would be generated. The energy transfer process of NaYF₄:Yb,Er and the FRET between it and Au using the energy level are shown in Fig. 6B. In fact, there is also a self-photothermal (from room temperature to 41.6 °C) of the

Au spheres solution at the wavelength of 980 nm, and the infrared thermal photograph is shown in Fig. S2, which may be caused by the local electronic field enhancement. The UCL spectra of NaYF₄:Yb,Er@Au-Pt(IV) and the following FA modified sample are shown in Fig. 6C. As shown, there is no great change among the three samples because there is almost no absorbance in the visible regions of Pt(IV) pro-drug and FA molecules. Photographs under daylight (left in each image) and the corresponding infrared thermal images (right in each image) of PBS, NaYF₄:Yb,Er-Pt(IV)-FA, and NaYF₄:Yb,Er@Au-Pt(IV)-FA solutions are shown in Fig. 6D, and the corresponding increased temperature curve is demonstrated in Fig. S3. As indicated, the solution of the final NaYF₄:Yb,Er@Au-Pt(IV)-FA sample after 5 min irradiation has the highest temperature (48.5 °C) compared with the PBS (36.7 °C) and NaYF₄:Yb,Er-Pt(IV)-FA without Au spheres modified (42.1 °C).

3.2 Biocompatibility, bio-imaging, and anti-cancer efficiency.

The proposed ideal Pt(IV) pro-drug and complex should have sufficient stability without decomposition in body fluid and blood stream, and good biocompatibility should be guaranteed before it reaches the cancer cell. Here, standard MTT assay was carried out to evaluate the short-term biocompatibility of the drug carriers (NaYF₄:Yb,Er@Au) and the Pt(IV) complex compared with the commercial used cisplatin. Before this, the amount of Pt(IV) carried on the NaYF₄:Yb,Er@Au was calculated by ICP-MS during the drug-loading process. Fig. 7A-D presents the viability of L929 cells incubated with concentrations of drug carrier from 15.63 to 500 µg mL⁻¹, and the corresponding concentrations of drugs range from 2.4 to 75 µg mL⁻¹. The viability of cells incubated with drug carrier NaYF₄:Yb,Er@Au of different concentrations is as high as 96.7%-112.4%. Even under the highest concentration of 500 µg mL⁻¹, there is still 100.6% of cells survived which indicates NaYF₄:Yb,Er@Au has no potential toxicity to normal cells. The viability of L929 cells incubated with the commercial drug cisplatin with different concentrations indicates that there is a stepped decreased viability from 94.1% to 30.4% with the concentrations increased from 9.4 µg mL⁻¹ to 75 µg mL⁻¹, this result indicates the conventional Pt(II) drugs may have serious side effect to normal cells of patients. While for Pt(IV) pro-drugs, the viability of cells is up to 87.2%-126.0% which indicates the small molecular platinum(IV) have no obvious inhibition to the normal cells. When the drug carrier was loaded with the nontoxic Pt(IV) pro-drugs, NaYF₄:Yb,Er@Au-Pt(IV) still keeps much higher viability (67.9%-101.8%) to normal cells compared with cisplatin. It seems there is cytotoxicity when the concentration is as high as 500 µg mL⁻¹ (67.9%). However, this concentration is much higher than the practical used amount.

Meanwhile, it is proposed that the clinical drugs and carriers should be steady in the bloodstream. Thus, the hemolysis properties of the clinical drugs of cisplatin, the drug carrier of NaYF₄:Yb,Er@Au, and NaYF₄:Yb,Er@Au-Pt(IV) complex are shown in Fig. 7E. The highest hemolytic efficiency of the three samples is 0.13%, 0.23%, and 0.22% with material concentration of 15.63-500 µg mL⁻¹ and the corresponding drug concentration of 2.4-75 µg mL⁻¹, indicating there is almost no hemolysis occurs to the drugs and materials.

Furthermore, the L929 cells incubated with 1 mg mL⁻¹ of NaYF₄:Yb,Er@Au and NaYF₄:Yb,Er@Au-Pt(IV) for 24 h and then dyed with DAPI and trypan blue. Compared with cells incubated with culture only, there is almost no dead cell

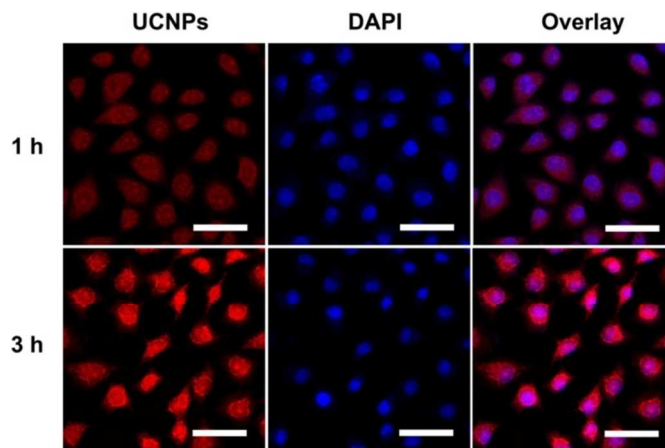


Fig. 8 Confocal laser scanning microscopy images of HeLa cells incubated with NaYF₄:Yb,Er@Au-Pt(IV)-FA for 1 h and 3 h. All the scale bars are 50 µm.

observed incubated with NaYF₄:Yb,Er@Au for 24 h (Fig. 7F, 7G), and there are few dead observed cells after incubated with NaYF₄:Yb,Er@Au-Pt(IV) for 24 h (Fig. S4). These results reveal that both of the drug carrier and the molecular drugs has no hemolysis to the human red cells, and as-synthesized Pt(IV) pro-drugs and complexes also have much better biocompatibility to the normal cells than that of the conventional cisplatin. Thus, although the cisplatin anticancer drug molecules are associated with higher reactivity for anti-cancer, the lower biological stability would limit its clinical application. For the candidate Pt(IV) pro-drug and complex with high biocompatibility and less injury to normal cells, they may have more extensive applications in anti-cancer field.

In order to achieve tumor targeting endocytosis to assure the anti-cancer therapeutic efficiency, NaYF₄:Yb,Er@Au-Pt(IV) was modified by FA molecules.⁵⁶ HeLa cells were seeded in the 6-well plated and incubated with the FA free and FA modified NaYF₄:Yb,Er@Au-Pt(IV) UCNPs for 3 h in the same condition at 37 °C with 5% CO₂. As shown in Fig. S5, the red channel is from the NaYF₄:Yb,Er@Au-Pt(IV) UCNPs which is excited at 552 nm for tracking the Pt(IV) complex, and the blue emissions (dyed by DAPI) is used to mark the nuclei. The red emissions may be caused by a non-irradiative or down-conversion process due to Yb,Er co-dopant (depicted in the energy level in Fig. 6B). The FA modified NaYF₄:Yb,Er@Au-Pt(IV) present stronger red luminescence than the cells incubated with particles without FA, suggesting more nanoparticles have been uptaken by HeLa cells. This result reveals there is a positive receptor-mediated endocytosis because of FA conjugation.

Fig. 8 presents the CLSM photographs of HeLa cancer cells incubated with NaYF₄:Yb,Er@Au-Pt(IV)-FA for 1 h and 3 h in to detect the cell uptaken process. The overlay of the two channels of red emissions from UCNPs and blue emissions from DAPI is shown correspondingly. In the initial 1 h, little red emission is found, indicating only a few of particles have been taken up by the cells, and stronger red fluorescence emission is found which suggests more particles are localized in the cells gradually. Meanwhile, we can see most of the red emissions focus in cytoplasm instead of in nuclei, indicating that NaYF₄:Yb,Er@Au-Pt(IV)-FA UCNPs have an endocytosis process instead of passive diffusion.

Yb doped particles can be used as contrast agents for CT imaging which is one of the most common clinic diagnostic

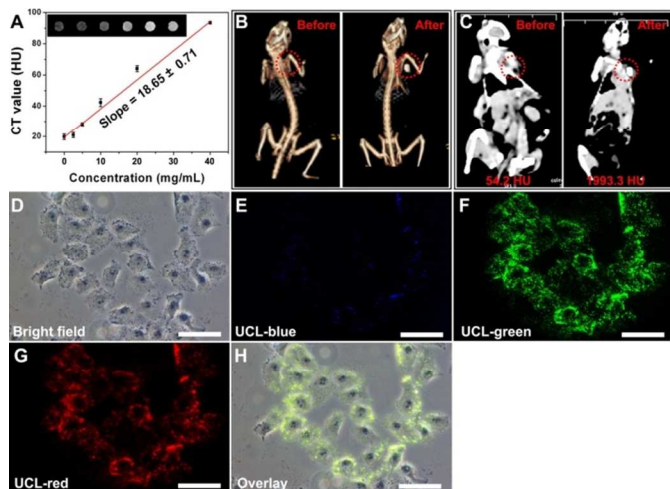


Fig. 9 (A) *In vitro* CT values as a function of the particle concentrations, (B, C) *in vivo* CT images before and after intratumoral injection. UCL microscopy images of HeLa cells incubated with NaYF₄:Yb,Er@Au-Pt(IV)-FA: (D) bright field, (E) blue region, (F) green region, (G) red region, and (H) overlay of the above channels under NIR irradiation. All the scale bars are 50 μ m.

techniques. Here, CT images of NaYF₄:Yb,Er@Au-Pt(IV)-FA UCNP *in vitro* and *in vivo* were performed. As shown in Fig. 9A, the CT signal increases obviously with enhanced concentration, and the values show high positive contrast enhancement as a function of the concentrations with a large slope of 18.64. The *in vivo* CT imaging of mice is shown in Fig. 9B and 9C, and the CT value in the tumor site is enhanced from 54.2 HU (Hounsfield units) to 1993.5 HU after injection. The high CT value indicates the platform could be used as CT imaging contrast agent for *in vitro* and *in vivo* imaging. Although the high resolution of CT imaging is important, there is a limitation because of low sensitivity, especially when it is used to tumor-imaging with small density differences. Fig. 9D-H present the inverted fluorescence microscope images of HeLa cells incubated with NaYF₄:Yb,Er@Au-Pt(IV)-FA UCNP (1 mg mL⁻¹). It is obvious NaYF₄:Yb,Er@Au-Pt(IV)-FA in the cells emits weaker blue and brighter green, red emissions upon 980 nm NIR irradiation. Also, UCL light are focused on the cytoplasm, which indicates the drug carriers are uptaken by endocytosis through inside endosomes and lysosome instead of passive adsorption.^{66,67} These dual-modal imaging properties reveal that UCNP are effective agents for real-time diagnosis.

The standard MTT assay and live/dead cell analysis to HeLa cells were employed to evaluate the anti-cancer therapeutic efficiency. The viability of HeLa cells incubated with the drug molecules of cisplatin, Pt(IV) pro-drug, NaYF₄:Yb,Er@Au-Pt(IV)-FA, and NaYF₄:Yb,Er@Au-Pt(IV)-FA under NIR irradiation is demonstrated in Fig. 10A. As seen, for the small molecular active cisplatin, the viability of cancer cells shows a concentration-dependent result, and only 29.7% of cells survive with the highest concentration of 75 μ g mL⁻¹. While for Pt(IV) pro-drugs, the viability is as high as 73.7%-111.5%, indicating the nontoxic character of small molecular Pt(IV). The reason for these different results between molecular cisplatin and Pt(IV) pro-drug is that Pt(IV) drugs could inhibit cell growth only in condition that they are reduced to Pt(II). A few of cancer cells are killed because some of the pro-drug molecules are reactive by the acid environment due to the characteristic cancer cells environment. While for NaYF₄:Yb,Er@Au-Pt(IV)-FA,

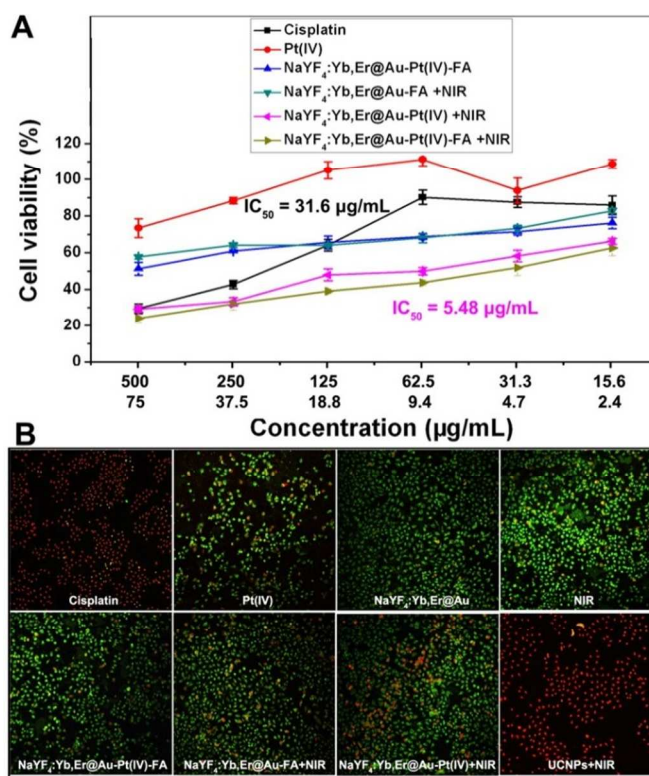


Fig. 10 (A) The cells viabilities of HeLa cancer cells incubated with separate small molecular cisplatin and Pt(IV) pro-drugs, with UCNP, with separate NaYF₄:Yb,Er@Au-FA, NaYF₄:Yb,Er@Au-Pt(IV) and with UCNP under NIR irradiation. (B) CLSM image of HeLa cells incubated with different groups. All the cells were marked with calcein AM and PI.

the viability of cancer cells have decreased a lot (51.5%-76.4%) compared with the molecular Pt(IV). The difference between Pt(IV) pro-drug and complex is caused by the different cell uptake process. As depicted above, the drug carriers enter the cells with endocytosis instead of passive diffusion. That means, the nanoparticles have priority to enter the early endosomes and late endosomes (pH 5.0-6.0), then coalesce with the lysosomes (pH 4.5-5.0) *via* endocytosis by cancer cells.⁶⁸ Additionally, FA improves the materials to recognize and enter the cancer cells through a receptor-mediated endocytosis. Under intracellular milieu, Pt(IV) pro-drug species could be reduced in this acidic micro environment to yield the cytotoxic Pt(II) molecules through eliminating the axial ligands reductively. As known, the obtained Pt(II) drugs reductive from the pro-drugs could kill about a half of cancer cells through DNA binding which seems not so satisfied.^{69,70} While for cells incubated with NaYF₄:Yb,Er@Au-FA (without Pt(IV) pro-drugs loaded) under NIR irradiation, there is only the photothermal effect, and the viability is 58.0% with the concentration of 500 μ g mL⁻¹. In order to improve the anti-cancer effect of NaYF₄:Yb,Er@Au-Pt(IV)-FA and simultaneously decrease the drug-resistance, photothermal effect is introduced with imaging guidance by the designed platform under NIR irradiation. As depicted in Fig. 6, there is obvious photothermal resulted due to the plastic resonance and FRET within the platform. After NIR laser irradiation, HeLa cells are restrained markedly with the survived cells ratio of 24.3%. Compared with that of NaYF₄:Yb,Er@Au-Pt(IV) (no FA) with NIR irradiation, the inhibition efficiency of NaYF₄:Yb,Er@Au-Pt(IV)-FA with NIR irradiation is higher which further indicated the targeting effect

of FA molecules. The IC_{50} value of cisplatin and $NaYF_4:Yb,Er@Au-Pt(IV)-FA+NIR$ is $31.6 \mu g mL^{-1}$ and $5.48 \mu g mL^{-1}$, respectively. This indicates there is a higher toxicity caused by the synergistic photothermal/chemo- effect than any single therapy.

Calcein AM (dyed living cells with green color) and PI (dyed dead cells with red color) were utilized to distinguish the live/dead state of HeLa cancer cells under different treatment conditions detected by CLSM (Fig. 10B). Here, the concentration of all the added nanoparticles is $1 mg mL^{-1}$ and the corresponding molecular platinum concentration is $150 \mu g mL^{-1}$. When there is cisplatin introduced, almost all of the cancer cells are killed due to the high inhibition effect with high dose of Pt(II) drugs. When there is small molecular Pt(IV) pro-drugs added, a few of cells are dead. When there is only $NaYF_4:Yb,Er@Au$ added, there is almost no dead cells appeared, and the NIR irradiation has no obvious inhibition to cancer cells. When there is only $NaYF_4:Yb,Er@Au-Pt(IV)-FA$ added without NIR irradiation, the inhibition effect is not so high as the MTT assay result in Fig. 10A which could be attributed to many premature dead cells washed away by PBS. This is the reason why MTT assay is essential. Additionally, when there is no chemo- effect of Pt(IV), part of cells incubated with $NaYF_4:Yb,Er@Au-FA$ under NIR irradiation for 5 min (pump power of $0.72 W cm^{-2}$) and more cells are killed for 10 min irradiation (Fig. S6). For the pump power of $1.44 W cm^{-2}$, almost no cells survive. However, the higher pump power may induce overheating which is not utilized in the clinical application. Meanwhile, without FA adjunct, the inhibition effect to the cancer cells incubated with $NaYF_4:Yb,Er@Au-Pt(IV)$ (no FA) with NIR irradiation is not so satisfied. Finally and amazingly, for the cancer cells incubated with the $NaYF_4:Yb,Er@Au-Pt(IV)-FA$ nanoparticles under NIR irradiation ($0.72 W cm^{-2}$), almost no cells survive which is even similar to the cisplatin cytotoxicity with high dose. There may be a synergistic effect because the high temperature could cause the irreversible destruction of the enzymes used in DNA synthesis and membrane integrity, while the Pt(II) could bind the DNA to avoid the cell passage, and this inhibition efficiency is obviously higher than that of individual chemo- or photothermal modal. In a sum, the high-biocompatible $NaYF_4:Yb,Er@Au-Pt(IV)-FA$ UCNPs have better anti-cancer therapeutic effect resulted from the synergistic photothermal/chemo- function (due to Au nanoparticles and Pt(IV) molecules), the special endocytosis (due to the drug carriers), and receptor-mediated effect (due to FA molecules) under NIR irradiation.

Conclusions

In summary, mesoporous 90-nm $NaYF_4:Yb,Er@Au-Pt(IV)$ anti-cancer platform was constructed by functionalizing PEI hydrogel, Au nanoparticles, and Pt(IV) molecules sequentially through physical attraction and chemical function conjunction. The finally conjugated FA is to achieve the receptor-mediated endocytosis to cancer cells. The results of MTT assay, hemolysis experiment, and live/dead cell analysis indicate that the as-synthesized $NaYF_4:Yb,Er@Au-Pt(IV)-FA$ has high biocompatibility, good up-conversion luminescence (UCL) imaging and CT imaging properties, and especially high anti-cancer efficacy. This may be caused by a synergistic photothermal/chemo- effect because the high temperature derived from the attached Au nanoparticles could cause the irreversible destruction of the enzymes used in DNA synthesis

and membrane integrity, while the attached Pt(II) could bind the DNA to avoid the cell passage.

Acknowledgements

Financial supports from the National Natural Science Foundation of China (NSFC 21271053, 21401032, and 51472058), Research Fund for the Doctoral Program of Higher Education of China (2011230411002), Natural Science Foundation of Heilongjiang Province (B201403), Harbin Sci.-Tech. Innovation Foundation (2014RFQXJ019) and Fundamental Research Funds for the Central Universities of China (HEUCF1412) are greatly acknowledged.

Notes and references

Key Laboratory of Superlight Materials and Surface Technology, Ministry of Education, College of Material Science and Chemical Engineering, Harbin Engineering University, Harbin 150001, P. R. China. E-mail: yangpiaoping@hrbeu.edu.cn; gaishili@hrbeu.edu.cn

† Electronic Supplementary Information (ESI) available: [TEM image and HRTEM image of Au NPs. Digital photograph and the infrared thermal image of Au NPs solution after NIR irradiation for 5 min. Temperature curves of the different solutions as a function of NIR irradiation time. Microscope images under the bright field and fluorescence field (405 nm) of L929 cells incubated with $NaYF_4:Yb,Er@Au-Pt(IV)$ dyed by DAPI and trypan blue. Microscopy images of HeLa cells incubated with $NaYF_4:Yb,Er@Au-Pt(IV)$ with and without FA modified for 1 h. CLSM images of HeLa cells incubated with $NaYF_4:Yb,Er@Au-FA$ under NIR irradiation for 10 min with different pump powers dyed by calcein AM and PI.]. See DOI: 10.1039/b000000x/

- 1 Y. S. Liu, D. T. Tu, H. M. Zhu, X. Y. Chen, *Chem. Soc. Rev.*, 2013, **42**, 6942-6958.
- 2 F. Wang, D. Banerjee, Y. Liu, X. Chen and X. Liu, *Analyst*, 2010, **135**, 1839-1854.
- 3 L. D. Sun, Y. F. Wang and C. H. Yan, *Acc. Chem. Res.*, 2014, **47**, 1001-1009.
- 4 D. T. Tu, L. Q. Liu, Q. Ju, Y. S. Liu, H. M. Zhu, R. F. Li, X. Y. Chen, *Angew. Chem. Int. Ed.* 2011, **50**, 6306-6310.
- 5 Z. Zhao, H. Fan, G. Zhou, H. Bai, H. Liang, R. Wang, X. Zhang and W. Tan, *J. Am. Chem. Soc.*, 2014, **136**, 11220-11223.
- 6 H. Xing, W. Bu, S. Zhang, X. Zheng, M. Li, F. Chen, Q. He, L. Zhou, W. Peng, Y. Hua and J. Shi, *Biomaterials*, 2012, **33**, 1079-1089.
- 7 Y. Wu, Y. Sun, X. Zhu, Q. Liu, T. Cao, J. Peng, Y. Yang, W. Feng and F. Li, *Biomaterials*, 2014, **35**, 4699-4705.
- 8 Y. Tao, E. Ju, Z. Liu, K. Dong, J. Ren and X. Qu, *Biomaterials*, 2014, **35**, 6646-6656.
- 9 J. Kim, Y. Piao and T. Hyeon, *Chem. Soc. Rev.*, 2009, **38**, 372-390.
- 10 Y. Sun, X. Zhu, J. Peng and F. Li, *ACS Nano*, 2013, **7**, 11290-11300.
- 11 C. Li, D. Yang, P. A. Ma, Y. Chen, Y. Wu, Z. Hou, Y. Dai, J. Zhao, C. Sui and J. Lin, *Small*, 2013, **9**, 4150-4159.
- 12 L. D. Carlos, R. A. S. Ferreira, V. d. Z. Bermudez, B. Julian-Lopez and P. Escribano, *Chem. Soc. Rev.*, 2011, **40**, 536-549.
- 13 A. D. Ostrowski, E. M. Chan, D. J. Gargas, E. M. Katz, G. Han, P. J. Schuck, D. J. Milliron and B. E. Cohen, *ACS Nano*, 2012, **6**, 2686-2692.
- 14 S. Zeng, Z. Yi, W. Lu, C. Qian, H. Wang, L. Rao, T. Zeng, H. Liu, H. Liu, B. Fei and J. Hao, *Adv. Funct. Mater.*, 2014, **24**, 4051-4059.
- 15 A. Hlavacek, A. Sedlmeier, P. Skladal and H. H. Gorris, *ACS Appl. Mater. Interface*, 2014, **6**, 6930-6935.
- 16 F. C. J. M. van Veggel, *Chem. Mater.*, 2014, **26**, 111-122.

- 17 Z. Chen, Q. Wang, H. Wang, L. Zhang, G. Song, L. Song, J. Hu, H. Wang, J. Liu, M. Zhu, *Adv. Mater.*, 2013, **25**, 2095-2100.
- 18 J. Liu, W. Bu, L. Pan and J. Shi, *Angew. Chem. Int. Ed.*, 2013, **52**, 4375-4379.
- 19 S. Zeng, M.-K. Tsang, C.-F. Chan, K.-L. Wong, B. Fei and J. Hao, *Nanoscale*, 2012, **4**, 5118-5124.
- 20 H. H. Gorris and O. S. Wolfbeis, *Angew. Chem. Int. Ed.*, 2013, **52**, 3584-3600.
- 21 X. Huang, S. Han, W. Huang and X. Liu, *Chem. Soc. Rev.*, 2013, **42**, 173-201.
- 22 L. Xia, X. Kong, X. Liu, L. Tu, Y. Zhang, Y. Chang, K. Liu, D. Shen, H. Zhao and H. Zhang, *Biomaterials*, 2014, **35**, 4146-4156.
- 23 F. Liu, Q. Zhao, H. You and Z. Wang, *Nanoscale*, 2013, **5**, 1047-1053.
- 24 J. V. Garcia, J. Yang, D. Shen, C. Yao, X. Li, R. Wang, G. D. Stucky, D. Zhao, P. C. Ford and F. Zhang, *Small*, 2012, **8**, 3800-3805.
- 25 R. P. Feazell, N. Nakayama-Ratchford, H. Dai and S. J. Lippard, *J. Am. Chem. Soc.*, 2007, **129**, 8438-8439.
- 26 S. Dhar, W. L. Daniel, D. A. Giljohann, C. A. Mirkin and S. J. Lippard, *J. Am. Chem. Soc.*, 2009, **131**, 14652-14653.
- 27 Y. Jung and S. J. Lippard, *Chem. Rev.*, 2007, **107**, 1387-1407.
- 28 P. M. Takahara, A. C. Rosenzweig, C. A. Frederick and S. J. Lippard, *Nature*, 1995, **377**, 649-652.
- 29 P. J. Bednarski, F. S. Mackay and P. J. Sadler, *Anti-Cancer Agents in Med. Chem.*, 2007, **7**, 75-93.
- 30 J. Turkson, S. M. Zhang, L. B. Mora, A. Burns, S. Sebti and R. Jove, *J. Biol. Chem.*, 2005, **280**, 32979-32988.
- 31 K. R. Barnes, A. Kutikov and S. J. Lippard, *Chemistry & Biology*, 2004, **11**, 557-564.
- 32 L. R. Kelland, C. F. Barnard, K. J. Mellish, M. Jones, P. M. Goddard, M. Valenti, A. Bryant, B. A. Murrer and K. R. Harrap, *Cancer Res.*, 1994, **54**, 5618-5622.
- 33 H. Xiao, G. T. Noble, J. F. Stefanick, R. Qi, T. Kiziltepe, X. Jing and B. Bilgicer, *J. Controlled Release*, 2014, **173**, 11-17.
- 34 W. J. Rieter, K. M. Pott, K. M. L. Taylor and W. Lin, *J. Am. Chem. Soc.*, 2008, **130**, 11584-11585.
- 35 Y. Min, J. Li, F. Liu, E. K. L. Yeow and B. Xing, *Angew. Chem. Int. Ed.*, 2014, **53**, 1012-1016.
- 36 W. Fang, S. Tang, P. Liu, X. Fang, J. Gong and N. Zheng, *Small*, 2012, **8**, 3816-3822.
- 37 X. Wang, C. Wang, L. Cheng, S.-T. Lee and Z. Liu, *J. Am. Chem. Soc.*, 2012, **134**, 7414-7422.
- 38 A. Kumar, S. Kumar, W.-K. Rhim, G.-H. Kim and J.-M. Nam, *J. Am. Chem. Soc.*, 2014, **136**, 16317-16325.
- 39 W. Chen, R. Yu, L. Li, A. Wang, Q. Peng and Y. Li, *Angew. Chem. Int. Ed.*, 2010, **49**, 2917-2921.
- 40 R. Lv, P. Yang, F. He, S. Gai, C. Li, Y. Dai, G. Yang and J. Lin, *ACS Nano*, 2015, **9**, 1630-1647.
- 41 X. Wang, K. Liu, G. Yang, L. Cheng, L. He, Y. Liu, Y. Li, L. Guo and Z. Liu, *Nanoscale*, 2014, **6**, 9198-9205.
- 42 L. Cheng, C. Wang and Z. Liu, *Nanoscale*, 2013, **5**, 23-37.
- 43 A. Priyam, N. M. Idris and Y. Zhang, *J. Mater. Chem.*, 2012, **22**, 960-965.
- 44 S. Xu, S. Xu, Y. Zhu, W. Xu, P. Zhou, C. Zhou, B. Dong and H. Song, *Nanoscale*, 2014, **6**, 12573-12579.
- 45 G. Wang, Q. Peng and Y. Li, *Acc. Chem. Res.*, 2011, **44**, 322-332.
- 46 J. Liu, J. Bu, W. Bu, S. Zhang, L. Pan, W. Fan, F. Chen, L. Zhou, W. Peng, K. Zhao, J. Du and J. Shi, *Angew. Chem. Int. Ed.*, 2014, **53**, 4551-4555.
- 47 L. Wang, H. Dong, Y. Li, C. Xue, L.-D. Sun, C.-H. Yan and Q. Li, *J. Am. Chem. Soc.*, 2014, **136**, 4480-4483.
- 48 J.-W. Oh, D.-K. Lim, G.-H. Kim, Y. D. Suh and J.-M. Nam, *J. Am. Chem. Soc.*, 2014, **136**, 14052-14059.
- 49 X. Chen, Y. Chen, M. Yan and M. Qiu, *ACS Nano*, 2012, **6**, 2550-2557.
- 50 M. A. Mahmoud and M. A. El-Sayed, *ChemCatchem*, 2014, **6**, 3540-3546.
- 51 M. Chen, S. Tang, Z. Guo, X. Wang, S. Mo, X. Huang, G. Liu and N. Zheng, *Adv. Mater.*, 2014, **26**, 8210-8216.
- 52 E. C. Dreaden, M. A. Mackey, X. Huang, B. Kang and M. A. El-Sayed, *Chem. Soc. Rev.*, 2011, **40**, 3391-3404.
- 53 H. Chen, X. Zhang, S. Dai, Y. Ma, S. Cui, S. Achilefu and Y. Gu, *Theranostics*, 2013, **3**, 633-649.
- 54 R. Lv, P. Yang, Y. Dai, S. Gai, F. He and J. Lin, *ACS appl. Mater. Inter.*, 2014, **6**, 15550-15563.
- 55 J. Yang, W. Liu, M. Sui, J. Tang and Y. Shen, *Biomaterials*, 2011, **32**, 9136-9143.
- 56 R. Lv, P. Yang, F. He, S. Gai, G. Yang and J. Lin, *Chem. Mater.*, 2015, **27**, 483-496.
- 57 H.-T. Wong, M.-K. Tsang, C.-F. Chan, K.-L. Wong, B. Fei and J. Hao, *Nanoscale*, 2013, **5**, 3465-3473.
- 58 Y. Dai, X. Kang, D. Yang, X. Li, X. Zhang, C. Li, Z. Hou, Z. Cheng, P. a. Ma and J. Lin, *Adv. Drug Deliv. Rev.*, 2013, **2**, 562-567.
- 59 K. Y. Lee, E. Seow, Y. Zhang and Y. C. Lim, *Biomaterials*, 2013, **34**, 4860-4871.
- 60 J.-C. Boyer, L. A. Cuccia and J. A. Capobianco, *Nano Lett.*, 2007, **7**, 847-852.
- 61 J. Zhao, Z. Lu, Y. Yin, C. McRae, J. A. Piper, J. M. Dawes, D. Jin and E. M. Goldys, *Nanoscale*, 2013, **5**, 944-952.
- 62 X. H. He and B. Yan, *J. Mater. Chem. C*, 2014, **2**, 2368-2374.
- 63 J. L. Zhuang, J. Wang, X. F. Yang, I. D. Williams, W. Zhang, Q. Y. Zhang, Z. M. Feng, Z. M. Yang, C. L. Liang, M. M. Wu and Q. Su, *Chem. Mater.*, 2009, **21**, 160-168.
- 64 F. Liu, X. He, L. Liu, H. You, H. Zhang and Z. Wang, *Biomaterials*, 2013, **34**, 5218-5225.
- 65 M. Haase and H. Schaefer, *Angew. Chem. Int. Ed.*, 2011, **50**, 5808-5829.
- 66 M. K. G. Jayakumar, A. Bansal, K. Huang, R. Yao, B. N. Li and Y. Zhang, *ACS Nano*, 2014, **8**, 4848-4858.
- 67 Q. He and J. Shi, *Adv. Mater. (Deerfield Beach, Fla.)*, 2014, **26**, 391-411.
- 68 D. Schmaljohann, *Adv. Drug Deliv. Rev.*, 2006, **58**, 1655-1670.
- 69 S. Dhar, Z. Liu, J. Thomale, H. Dai and S. J. Lippard, *J. Am. Chem. Soc.*, 2008, **130**, 11467-11476.
- 70 A. C. Plooy, M. van Dijk and P. H. Lohman, *Cancer Res.*, 1984, **44**, 2043-2051.